



Superconducting toroidal combined-function magnet for a compact ion beam cancer therapy gantry

D.S. Robin^{a,*}, D. Arbelaez^a, S. Caspi^a, C. Sun^a, A. Sessler^a, W. Wan^a, M. Yoon^{a,b}

^a Lawrence Berkeley National Laboratory, 1 Cyclotron Road, Berkeley, CA 94720, USA

^b Department of Physics, Postech, Hyoja-dong, Pohang, Gyeongbuk 790-784, Republic of Korea

ARTICLE INFO

Article history:

Received 31 May 2011

Received in revised form

2 August 2011

Accepted 25 August 2011

Available online 14 September 2011

Keywords:

Carbon gantry

Hadron therapy

Gantry beam optics

Superconducting magnets

ABSTRACT

A superconducting, combined-function, 5 T, 90°, toroidal magnet with a large bore is described in this paper. This magnet is designed to be the last and most difficult part of a compact superconducting magnet-based carbon gantry optics for ion beam cancer therapy. The relatively small size of this toroidal magnet allows for a gantry the size of which is smaller or at least comparable to that of a proton gantry. The gantry design places the toroidal magnet between the scanning magnets and the patient, that is the scanning magnets are placed midway through the gantry. By optimizing the coil winding configuration of this magnet, near point-to-parallel optics is achieved between the scanning magnets and the patient; while at the same time there is only a small distortion of the beam-shape when scanning. We show that the origin of the beam-shape distortion is the strong sextupole components, whose effects are greatly pronounced when the beam is widely steered in the magnet. A method to correct such an undesirable effect is suggested and demonstrated by a numerical particle tracking through the calculated three-dimensional magnetic field.

© 2011 Elsevier B.V. All rights reserved.

1. Introduction

In an accelerator based ion-beam particle therapy (IBT) facility, ions (typically protons and carbon ions) are accelerated and injected into patients' bodies to treat deep-seated cancer tumors. Many IBT facilities use rotatable gantry beamlines to direct the ion-beam at the patient from different angles. The ability of gantries to direct the beam into the body from different angles allows for using the combination of angles that will minimize the radiation dose to healthy tissue. As a result, many multi-room proton-only IBT facilities have equipped the majority of their treatment rooms with gantries.

Gantries, however, are expensive, requiring large (4–7 m radius) structures enclosed in large, heavily shielded rooms. This is particularly true for carbon treatment facilities. The reason being that carbon ion beams require higher beam energies and a factor of two difference in charge to mass ratio and are thus larger facilities than proton beams. For an IBT facility, the typical penetration depth range desired is 3–30 cm. To reach 30 cm depth in water requires a carbon beam of 430 MeV/u versus only 220 MeV for proton beams. To achieve a 30 cm penetration depth,

the magnetic rigidity of a 430 MeV/u carbon ion is approximately 2.5 times higher than a 220 MeV for proton ion.

At present there are many proton beam gantries in operation, however, there exists only one gantry for carbon beams. This is at the newly built Heidelberg Ion Therapy (HIT) facility [1,2]. As compared with an equivalent proton gantry (for example the state-of-the-art Gantry-II at the Paul Sherrer Institute (PSI) [3]) the HIT gantry is roughly 50% larger and five times heavier. The HIT gantry size is 22 m long by 14 m high and weighs more than 600 t. It is unlikely that many facilities will be able to afford multiple carbon gantries of the size and weight of the HIT gantry.

For both the HIT gantry and PSI Gantry-II, the size and weight is driven by the final large aperture 90° magnet of their gantries. In this paper we present a coil winding concept for a large aperture, combined-function 90° magnet that allows for a significantly more compact carbon ion gantry. The winding concept enables the reduction in the size and weight of the magnet without compromising the important beam transport properties. With a superconducting gantry, consisting of small bore magnets followed ultimately by the magnet discussed in this paper, it may be possible to realize a carbon gantry with comparable size and weight as that of PSI Gantry-II.

In Section 2 we outline the main desirable properties of gantries. In particular we discuss active scanning, size of the good field region, source-to-axis distance, and scanning speed. We present the current state-of-the-art for active scanning gantries

* Corresponding author.

E-mail address: dsrobin@lbl.gov (D.S. Robin).

that exist at PSI Gantry-II for protons and HIT for carbon, respectively. We show that they are both derivatives of the same design and require a large aperture final bend. This large aperture bend drives the size, weight, and cost of the gantry and treatment rooms. In Section 3 we discuss the requirements of the large aperture final dipole including linear and nonlinear fields required for the large aperture magnet to allow for parallel scanning at the patient. In Section 4 we discuss the possibility of using large superconducting toroidal aperture combined-function magnet based on tilted solenoidal pairs to reduce the size and weight of the final bend. In Sections 5 and 6 we present the coil design, optimization, and beam transport simulations. Finally in Section 7 we conclude and discuss future directions.

2. Desirable gantry properties and the present state-of-the-art

The present state-of-the-art of gantries are very advanced. Many gantries rotate about the patient that together with horizontal patient rotation provide full 4π coverage. In minimizing the dose to healthy tissue, the treatment planner picks several angles (typically 2–4) for delivering the beam. At each angle, the gantry magnets and the patient are fixed in space and the beam is scanned over the tumor. The most advanced scanning gantries in operation are PSI Gantry-II for protons and the HIT gantry for carbon. These gantries provide at each gantry angle rapid, parallel, active “pencil beam” scanning over large transverse fields. They are both derivatives of the same design concept [5] (which we refer to as the Pavlovic type design) that is shown in Fig. 1. We now elaborate on a few of the features provided by these gantries.

Active scanning refers to a type of ion beam delivery where a small “pencil” sized ion beam is scanned over the tumor volume in all three dimensions (two transverse and depth). Scanning the transverse direction is achieved using fast scanning magnets and the depth change is made by changing the particle beam energy. Active scanning is desirable because it allows for optimal conformation to the tumor shape.

At each gantry position, the three-dimensional scanning of the beam on the tumor is completed within a few minutes. The most advanced proton scanning gantry is at PSI Gantry-II where the gantry has been designed to make one 3D painting of a cubic liter tumor in about 6 s. This allows for several repaintings within a minute. For the HIT gantry one painting takes longer—on the order of a minute.

The good field region is defined as the size of the transverse region that can be scanned without moving the patient table. If the tumor is larger than the good field region, scanning the entire tumor requires moving the patient table. In such a case the “fields” need to be “stitched” together. This is time consuming and introduces potential errors. The larger the good field region, the fewer number of tumors that require stitching. However,

increasing the size of the good field region has consequences on the size and complexity of the gantry. So there needs to be a compromise. One recent survey in Europe [4] concluded that the minimum acceptable good field region is 225 cm^2 . The good field region for the PSI Gantry-II is $12 \times 20 \text{ cm}^2 = 240 \text{ cm}^2$ and the good field region for the HIT gantry is $20 \times 20 \text{ cm}^2 = 400 \text{ cm}^2$.

The beam scanning can be made parallel or with an angle. In the case of parallel scanning, scanning the beam results in the beam being shifted in a parallel manner, i.e., there is no change in the beam angle with scanning. With angular scanning the beam direction does not remain parallel when the beam is scanned. Parallel scanning has some advantages in reducing the complexity of field patching and dosimetry.

2.1. Large aperture final bend

In the case of PSI Gantry-II and the HIT gantry, the scanning magnets are placed upstream of the last 90° bend magnet. The scanning magnets deflect the beam. The angular deflection at the scanning magnets translates to a position offset at the patient. The offset is purely position and there is no angle—in other words parallel scanning. To achieve parallel scanning, the linear magnet optics between the scanning magnets and the patient requires careful design. This is accomplished by adjusting the horizontal and vertical transverse focusing of the bend. In the case of both HIT and PSI Gantry-II, this focusing is obtained by rotating the initial (IR) and exit (ER) edge angles of the bend (see Fig. 1).

The attraction of this concept is that it is a relatively radially compact gantry with parallel scanning. A main drawback of this concept is the final 90° magnet needs to have a wide aperture in both transverse directions to accommodate the large beam displacements while the beam is being scanned. As a result this magnet is considerably larger and heavier than any of the other elements in the beamline, and drives the size and weight of the gantry and the room. In the case of HIT, the weight of the 90° magnet is 90 t which is 65% of the weight of the entire rotating transfer system [1,2].

This problem is not unique to fixed isocentric gantries but any gantry where the scanning magnets are located upstream of the final bend. This is the motivation for exploring large aperture magnet concepts with smaller size and weight. Next we will summarize the requirements for the large aperture magnet and then discuss our approach using superconducting tilted solenoids wound on a torus.

3. Requirements of a large aperture final bend

There are several functional requirements of a final bend of a gantry where the scanning magnets are located upstream of the final bend.

- Large aperture to accommodate the scanned beam.
- Bend the beam by a large angle.
- Enable point-to-parallel focusing from the scanning magnets to the patient.
- Minimize beam-shape distortion when scanning the beam.
- Quickly ramp the field.

The first requirement of the large aperture is necessary to accommodate the scanned beam inside the magnet. The next three requirements determine the basic specifications for the magnetic field. From these requirements we see that the desired fields are not necessarily that of a pure dipole.

The second requirement, the bending angle requirement, depends upon the layout of the gantry. In the Pavlovic type

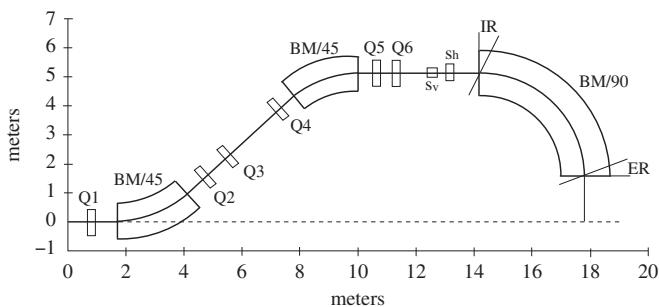


Fig. 1. Magnetic layout of the Pavlovic type gantry with bending magnets (BM), quadrupole magnet (Q), horizontal and vertical scanning magnets (Sv and Sh).

gantry, the bending angle is 90° but it could be different in other gantries. The bending radius is determined by the ion momentum and the strength of the magnetic field.

The third requirement, the point-to-parallel requirement, is derived from the desire to have parallel scanning (as discussed in the previous section). This is achieved by introducing focusing in the bend by either adjusting the bend edge angles (as shown in Fig. 1) or by adding a gradient field to the body of the magnet to make the beam parallel at the patient. In other words, the linear transfer function from the scanning magnets to the patient is adjusted to be point-to-parallel.

The fourth requirement of minimizing the beam-shape distortion while scanning is important to ensure that it is possible to accurately deliver the required dose distribution to the tumor volume in a controlled way. This becomes more difficult if the beam distribution becomes too distorted, then it becomes harder to achieve this. To satisfy this requirement, the transfer map of the beam trajectory between the scanning magnets to the patient position should not have large nonlinear terms. This in turn requires that the nonlinear magnetic fields in the magnet be properly adjusted.

The final field ramping requirement is derived from the desire to scan the beam energy over a large range—from 3 cm to 30 cm. In the case of the PSI Gantry-II, the time to change a 5 mm in depth is less than 100 ms. In the case of the HIT gantry, the gantry is also capable of making a 5 mm step in 100 ms but the synchrotron is limited to about 4 s.

4. Large aperture, tilted superconducting solenoidal pair, combined-function bend

4.1. Basic concept

Superposing two solenoid-like thin windings that are oppositely skewed (tilted) with respect to a cylindrical axis, the combined current density on the surface is $\cos \theta$ -like and the

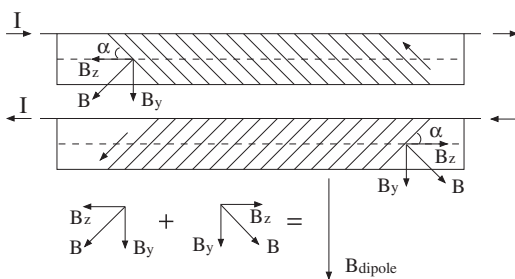


Fig. 2. Superposition of two alternating skewed solenoids generating a perfect dipole field.

resulting magnetic field in the bore is a pure dipole. Good field quality in the straight section is achieved without optimization (no wedges) [16] and over the magnet ends harmonics naturally integrate to zero [17,18]. The simplicity of this design, void of typical wedges, end-spacers, and coil assembly is especially suitable for low cost superconducting accelerator magnets. We report here on the extension of the concept by placing the windings on a toroidal geometry suitable for a curved magnet.

4.2. History of this concept

In a published paper by Meyer and Flasck in 1970 [6], the authors discussed the magnetic field resulting from the superposition of two oppositely skewed (tilted) solenoids with respect to the bore axis (see Fig. 2). If two layers are perfectly superposed (at the same radius) the current density cancels its azimuthal component and doubles its axial one resulting in a superimposed field that nulls the solenoid component and doubles the dipole strength. Each discrete turn of the tilted solenoid winding lies on an elliptical plane and generates an equivalent current density that is proportional to thus assuring the pure nature of the dipole field. This original concept gained renewed interest in the past few years [7–15] partially for use as insert coils in high field Nb_3Sn magnets [11,12] and partially as stand alone accelerator magnets.

In 2005 the concept was demonstrated on a small bore superconducting NbTi dipole magnet that was built and tested as part of a summer student program at LBNL. Impressed by the design simplicity and low construction cost the concept was extended a year later towards the construction of a similar quadrupole magnet. Advantages of this concept are as follows: (1) high field quality over an extended dynamic range, (2) no field optimization required, (3) small number of components—wedges and spacers not needed, (4) coil assembly not needed (all poles are wound together around a single bore), (5) small bore sizes not limiting $\cos \theta$ -like windings, (6) continuous windings and ease of magnet grading.

4.3. Extension to a toroid

Applying the winding concept to the construction of toroidal coils has the benefit of eliminating difficulties in placing windings, under tension, over a concave surface. Placing windings under tension on the inner radius of a torus poses a technical challenge in the way windings are held, special tooling may thus be required to assure the proper position of each turn (Fig. 3). The present technique maintains winding tension on both the inner and outer surface of the torus thus controlling the winding process and reducing the coil size. The net benefit is a magnet that is more compact, cost effective and better positioned to



Fig. 3. Top view of windings on a torus following a concave path (left) and a convex path (right). Tension on the windings can only be maintained along the convex path.

handle the large Lorentz forces that develop during operation. We show in particular that it is possible to arrive at a combined-function winding geometry where the resulting multipole field content can satisfy all the aperture and field constraints of the final bend (see Section 6) of a carbon ion gantry.

5. Initial coil design

We examined a number of different winding schemes on a torus. We chose the size of the inner bore radius to be 10 cm. This inner radius size was chosen to accommodate a good field region area greater than 225 cm². In the case of a circular good field region, the good field region's radius extends to 8.5 cm or 85% of the inner bore radius. The large ratio of 85% resulting from such a

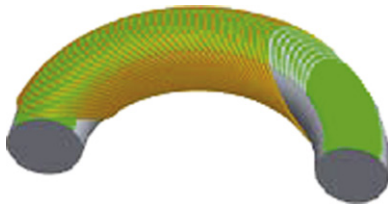


Fig. 4. Drawing showing initial coil design concept with the coils touching the inner radius. They also touch on the outer radius.

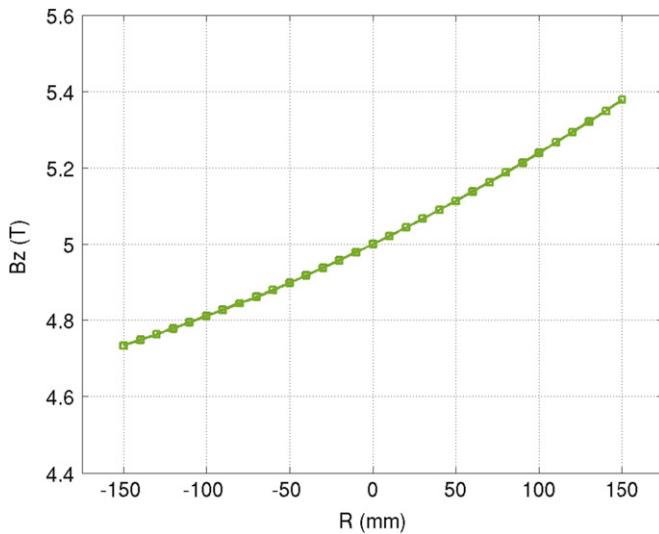


Fig. 5. Field gradient along the mid plane for the initial winding scheme. Field is 5 T at the center of the toroid with a field gradient of 2.4 T/m.

small bore size was made to balance several competing effects. On one side it is important to reduce the bore size because the magnet's weight, stored energy, and stresses all increase with increasing bore radius. However, the bore radius should not be too close to the good field region so that distortions in the magnetic field create distortions in the beam while scanning. We show in Section 6.3 that the resulting distortion can be made small.

Initially a compact winding scheme was chosen that requires each turn to remain in contact with its neighboring turns on the mid-plane of both the inner radius and outer radius of the torus but not elsewhere (see Fig. 4). A computer program that places wires along such a path was written to calculate the magnetic field using Biot–Savart law. The coil windings have also been integrated into OPERA-3D for additional calculations including the use of ferromagnetic material. Such a winding scheme resulted in the vertical field increasing at larger radius (see Fig. 5). This positive field gradient is not ideal to meet the parallel-to-point requirement in both planes. The reason is that the magnet is sector bend like so the edge angles provide horizontal focusing and with little vertical focusing. With the addition of the positive field gradient, the magnet becomes vertically defocussing. However, there should be a negative gradient so that the combination of edge focussing and negative gradient provides net focussing in both the horizontal and vertical plane. To meet this condition we determined that the field

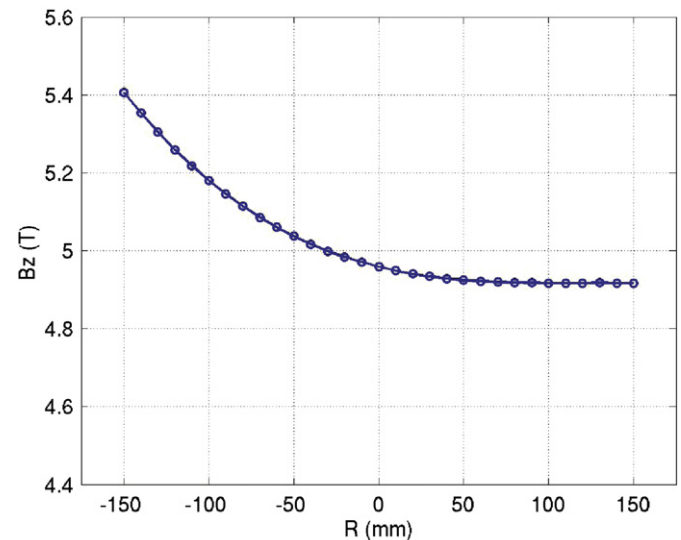


Fig. 7. Field gradient along the mid plane of the initial winding with iron.

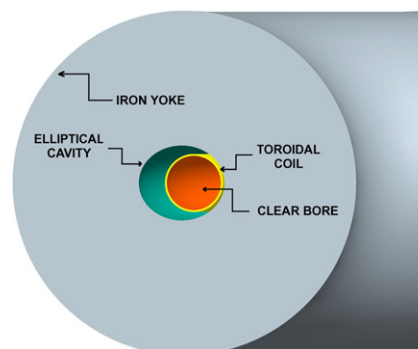
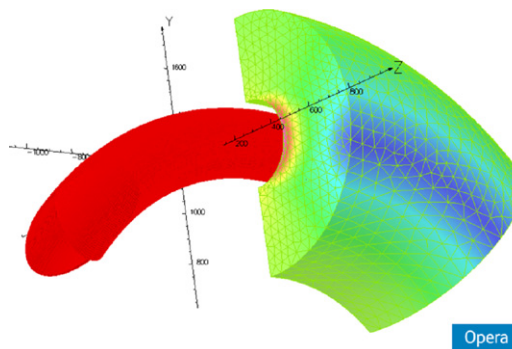


Fig. 6. Drawing of an elliptically shaped iron placed asymmetrically around the coils. The figure on the left is a 3D drawing generated by software OPERA and the figure on the right is a 2D drawing.

gradient in the magnet should have a value that is 2.26 T/m (roughly equal and opposite to that in Fig. 5).

In an attempt to reverse the field gradient an elliptically shaped iron toroid shown in Fig. 6 was placed asymmetrically around the coils with more iron closer to the inner radius and further from the outer radius. Doing this did indeed change the gradient. In the middle of the magnet the linear field gradient of -1.06 T/m was obtained. However, a second order (sextupole) gradient term of 9.03 T/m² was added (see Fig. 7). We quickly realized that it is extremely difficult to manipulate the high order field components using iron, which have to be optimized by the winding. Nevertheless, this attempt was the initial case in which properties of the beam dynamics was studied.

5.1. Particle tracking and beam shape distortion

To evaluate the effect of scanning and beam distortion, simulations were carried out where particles were tracked from the entrance of the gantry to the patient position for different settings of the scanning magnets. The following procedure was followed.

First we assumed a Pavlovic type isocentric gantry design [5] similar to that used in PSI and HIT. However, in this design the field strengths of the 45° and 90° bends were 5 T. The resulting gantry size is about 9.97 m long by 3.12 m high, which is slightly smaller than the size of PSI Gantry-II.

For the initial conditions we made the following assumption. Emittances at the gantry entrance are chosen to be 1 mm mrad (horizontal) and 5 mm mrad (vertical) and the momentum spread be 0.2%, which are typical values for a beam extracted from carbon synchrotron [6]. Six quadrupoles (see Fig. 1) are then utilized to achieve a matched solution at the position of the patient, which is 1.9 m distance apart from the exit of the 90° bending magnet. The matching constraints are $R_{11} = R_{33} = 0$ for rotation-independent optics, $R_{16} = R_{26} = 0$ for achromat condition, and $X = R_{12} \sqrt{\sigma(0)_{22}}$, $Y = R_{34} \sqrt{\sigma(0)_{44}}$ for output beam size control, where R_{ij} is the ij component of the 6×6 linear R matrix, X (Y) is the horizontal (vertical) beam size at the patient position, $\sigma(0)_{22}$ ($\sigma(0)_{44}$) is the horizontal (vertical) beam divergence at the gantry entrance. For rotation-invariant optics these input divergence angles must be the same (see Ref. [5]). Thus, at least six quadrupoles are required to get a solution which satisfies all of these six constraints.

For ± 2 mm beam spot at the target, the initial beam sizes are taken to be 2 mm and 10 mm in the horizontal and vertical plane, respectively and the divergence angle is 0.5 mm mrad in both planes. Total 1000 particles are Gaussian-distributed in phase space. The phase-space coordinates for these particles are then linearly transformed to the position of scanning magnets where the program for numerical integration of the equations of motion is invoked to track the particles to the position of the patient. The calculated fields from OPERA-3D are saved and read by a numerical particle tracking program which solves the Lorentz equation in cylindrical coordinates with the azimuthal angle as an independent variable. The equations expressed in cylindrical coordinates (ρ, ϕ, z) are

$$\rho' = \frac{d\rho}{d\phi} = \frac{d\rho}{dt} \frac{dt}{d\phi} = \frac{\rho v_\rho}{v_\phi}$$

$$z' = \frac{dz}{d\phi} = \frac{dz}{dt} \frac{dt}{d\phi} = \frac{\rho v_z}{v_\phi}$$

$$v'_\rho = \frac{dv_\rho}{d\phi} = v_\phi + \frac{q\rho}{\gamma m} \left(B_z - \frac{v_z B_\phi}{v_\phi} \right)$$

$$v'_z = \frac{dv_z}{d\phi} = \frac{q\rho}{\gamma m} \left(\frac{v_\rho}{v_\phi} B_\phi - B_\rho \right) \quad (1)$$

where $v_\phi (= \sqrt{v^2 - v_\rho^2 - v_z^2})$ the azimuthal component of the particle velocity, q the particle charge, m the rest mass, γ the usual relativistic factor, and B_α is the α th component of the magnetic field.

These equations are solved by the fourth-order Runge–Kutta method. Tracking is performed by invoking three-dimensional interpolation of fields. To facilitate the computing time, only those fields (usually 11 points in each direction) adjacent to the present particle position are utilized for the interpolation.

The beam is deflected at various angles at the position of steering magnets (Fig. 8) so ideally the beam centroids must show a linear dependence on kick angles while at the same time the shape of the beam should not change. Fig. 9 shows the beam spots in the transverse plane at the patient position for initial design of the 90° magnet. This figure shows a large distortion of the beam shape and also significant deviation from linearity. This is considered mainly due to large sextupole components in the main body of the magnet.

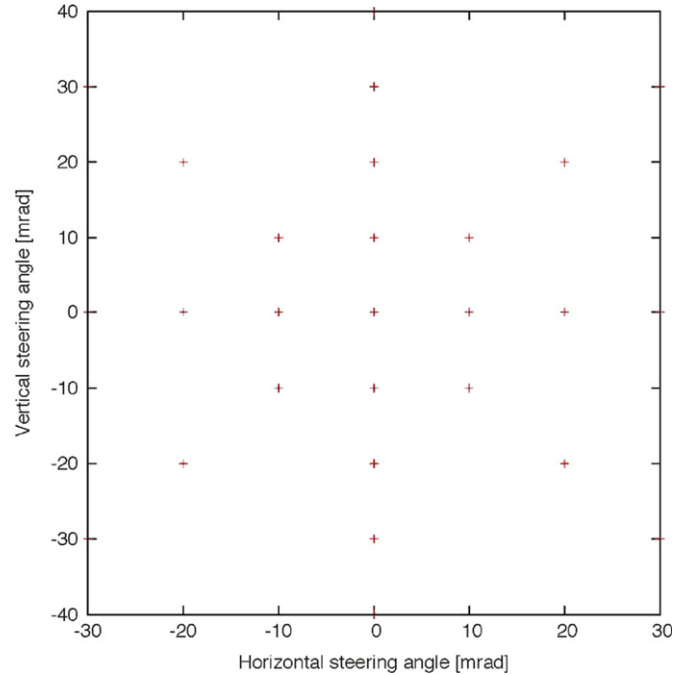


Fig. 8. Horizontal and vertical scanning magnet settings.

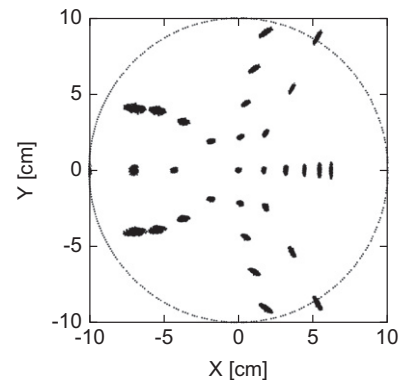


Fig. 9. Beam shapes at the patient position with initial winding with iron.

Treating a sextupole as a thin lens, we have expressions for kicks due to a sextupole magnet as

$$\Delta x' = -\frac{k_2 l_s}{2}(x^2 - y^2), \quad \Delta y' = k_2 l_s xy \quad (2)$$

where $k_2 = B''/B\rho$ is the normalized sextupole strength with $B\rho$ being the magnetic rigidity of a particle and l_s is the magnetic length of the sextupole. Fig. 9 can be understood easily from these equations. For example, along the $x=0$ line, $\Delta x' \propto k_2 y^2$ and is always positive regardless of the sign of y when k_2 is positive while $\Delta y' = 0$. As a result, the distortion shown in Fig. 9 is expected. Similarly along the $y=0$ line, $\Delta x' \propto -k_2 x^2$ and is always negative regardless of the sign of x when k_2 is positive while $\Delta y' = 0$. Behaviors along the diagonal direction can be explained by a similar manner. This shows that it is necessary not only to correctly determine the optimal linear and nonlinear field values, but also to design the magnet to obtain these field components.

6. Winding optimization

The Differential Algebra (DA) code COSY INFINITY [19] is used to model the magnetic field generated by the initial winding scheme, and this magnetic field model is further used to study its beam dynamics. The study showed that the required dipole field B_0 is about 5.0 T in the middle of the torus, and required quadrupole B_1 and sextupole B_2 gradients are -2.26 T/m and 1.30 T/m², respectively (see Fig. 10). The small, but non-zero, sextupole was found to help balance out the sextupole terms arising from the fringe field. To generate such required magnetic fields, we need to know how to wind the coil on the torus. Several algorithms, such as maximum likelihood, rand walk and Genetic optimization, can be used to find optimal winding solutions. However, the Genetic Algorithm is considered as the most suitable method for this multi-variable and multi-objective optimization problem, because it not only can perform a global optimal search, but also can generate multiple solutions with trade-offs among the optimization objectives. Details of this Algorithm will be discussed later.

6.1. Winding parametrization

Using optimization algorithms to search for winding solutions, first we need to parameterize the winding path of the coil on the

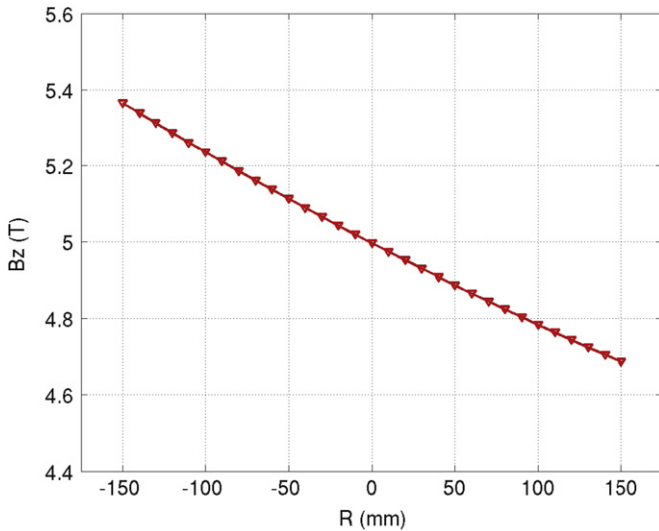


Fig. 10. Field gradient along the mid plane for an ideal field. Field is 5 T at the center of the toroid with a field gradient of -2.26 T/m.

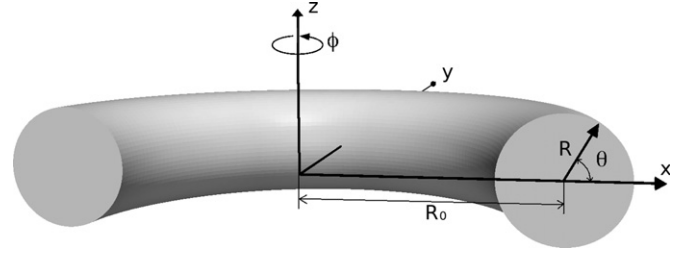


Fig. 11. Simple toroidal coordinate system. R_0 and R are the major and minor radius of the torus, respectively; ϕ is the toroidal angle and θ is the poloidal angle. The origin of the Cartesian coordinate system (x, y, z) is at the center of the torus.

surface of torus. To simplify the description of the winding, the simple toroidal coordinate system (R, ϕ, θ) is used, where R is the radius of the torus bore (called minor radius), ϕ is the toroidal angle and θ is the poloidal angle shown in Fig. 11. The simplicity of using this coordinate system is the result of that the constant R forms the surface of the torus. Therefore, we only need two parameters ϕ and θ to describe the winding.

Given the bore radius R , the relationship between ϕ and θ , i.e., $\phi = f(\theta)$, will determines the winding path of the coil on the surface of the torus. Now the question arises: what kind of winding relation $\phi = f(\theta)$ generates not only the dipole field but also the quadrupole and sextupole fields. It has been well known that for a straight cylinder the $\cos \theta$ -like current distribution on the cross-section of the cylinder will generate multipole fields, i.e., $\cos \theta$ gives dipole field, $\cos 2\theta$ gives quadrupole field, and so on. Similarly, we propose the following winding relation for torus:

$$\phi = \theta/n + a_0 \sin \theta + a_1 \sin 2\theta + a_2 \sin 3\theta + \dots \quad (3)$$

where n is the coefficient determining the number of turn of the coil on a 2π torus, and a_0, a_1, a_2, \dots determine the multipole field components. If the main field is dipole field, the coefficient a_0 will be much larger than a_1 and a_2 . In this case, the tilt angle α of the coil with respect to the torus bore axis as shown in Fig. 2 mainly depends on the coefficient a_0 . The larger the coefficient a_0 is, the smaller the tilt angle.

To calculate the magnetic field due to the winding path given by Eq. (3), however, it is convenient to transform the winding description from the toroidal coordinate system (R, θ, ϕ) to Cartesian coordinates (x, y, z) . The coordinate transformation between them is given as follows:

$$x = (R_0 + R \cos \theta)A \cos \phi$$

$$y = (R_0 + R \cos \theta)A \sin \phi$$

$$z = R \sin \theta \quad (4)$$

where R_0 is the radius of the spine of torus, called major radius (Fig. 11). Thus, for given coefficients n, a_0, a_1, a_2, \dots as well as the coil current I , the magnetic field inside the torus can be numerically evaluated using Biot–Savart law.

6.2. Genetic optimization

Now, the question is what values the coefficients n, a_0, a_1, a_2, \dots and current I should be in order to generate required magnetic field. To solve this problem, Genetic Algorithms (GA) are applied.

Concisely stated, Genetic Algorithm is a method to find solutions by mimicking the process of natural evolution, such as inheritance, mutation, selection and crossover. The details of this algorithm can be found in Ref. [20]. Given a specific problem to solve, the implementation of GA begins with a set of trial solutions (called population) which are typically randomly generated. Then, the merit

functions (the fitness or objective functions) of these trial solutions are quantitatively evaluated. According to their fitnesses, the promising candidates are kept and used to reproduce a new population using crossover operator. To diversify the population, usually mutations are introduced during the reproduction. This is motivated by a hope that the new generation will be better than the old one. It is repeated until the maximum number of generation is reached or the optimal solutions are found. Genetic Algorithms have proven to be an enormously powerful and successful multi-variable and multi-objective problem solving strategy, and have been used in a wide variety of fields.

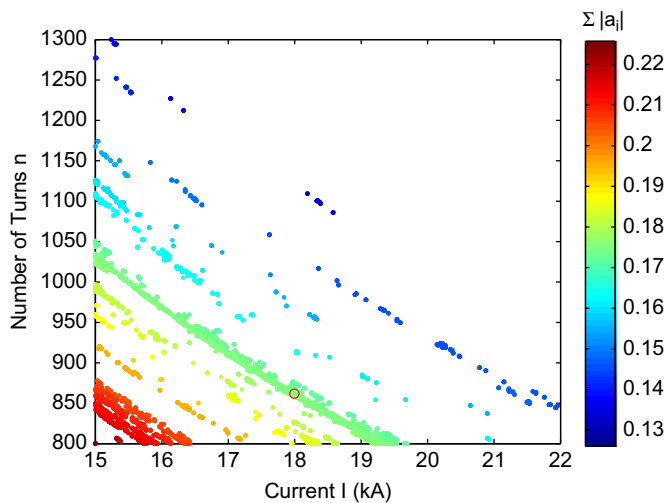


Fig. 12. Winding solutions with trade-offs among the coil current I , the number of winding turn n , and the amplitude of the coefficients $\Sigma|a_i|$. The circle indicates the solution presented in the text.

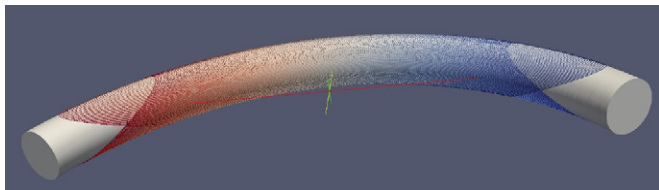


Fig. 13. A winding solution. The minor radius of the torus is 10.5 cm and the major radius is 126.9 cm.

Using GA to solve the winding parameters n, a_0, a_1, a_2 and I for given magnetic field, the differences between the calculated multipole field strength and the required ones are used as optimization constraints which need to satisfy the field requirement, and the winding current I , the number of winding turns n and the amplitude of the coefficients a_0, a_1, a_2 are used as the optimization objectives which are minimized during the optimization process.

The solutions with trade-offs among I, n and $\Sigma|a_i|$ after 500 generations are shown in Fig. 12. The population size of 20 000 is used for this problem. The calculation took about 50 h with 64 CPUs using the high performance computing cluster Lawrenceium at Lawrence Berkeley National Laboratory [21]. All the solutions shown in Fig. 12 meet the field requirements, and the trade-offs among the current I , and number of winding turn n and coefficient amplitude $\Sigma|a_i|$ can be clearly seen. A low current solution requires more winding turns if the tilt angle of the coil remains the same, and less winding turns and low current solution requires a small tilt angle (i.e., large amplitude of the coefficients $\Sigma|a_i|$).

One of these solutions indicated in Fig. 12 is given here

$$I = 18 \text{ kA}, \quad n = 864, \quad a_0 = 0.168$$

$$a_1 = -5.74 \times 10^{-3}, \quad a_2 = 2.345 \times 10^{-4}.$$

The current though one coil cable is 18 kA, and the number of winding turn on 2π torus is 864. Fig. 13 shows the winding path of this solution on the torus. The magnetic field of this winding across the bore of the torus is shown in Fig. 14, which clearly meet the requirements. A rough estimation shows that this magnetic field is under 80% of the critical field of the superconductor.

The solution presented is only one possible solution that meets the field requirements. There are many others with different combination of (I, n, a_0, a_1, a_2) values. This allows us to explore different options and choose those which are most practical (i.e., easier to wind, lower tolerances, lower stress and stored energy, etc.).

Note that a simple coil model has been assumed in the optimization, i.e., the thickness of the conductor, the insulation and the gap between two layers of the conductors are not taken into account. However, in reality, to calculate the current density we assume an “engineering” value that includes the thickness and insulation of the conductor. The optimization with a more realistic conductor model will be implemented in the near future.

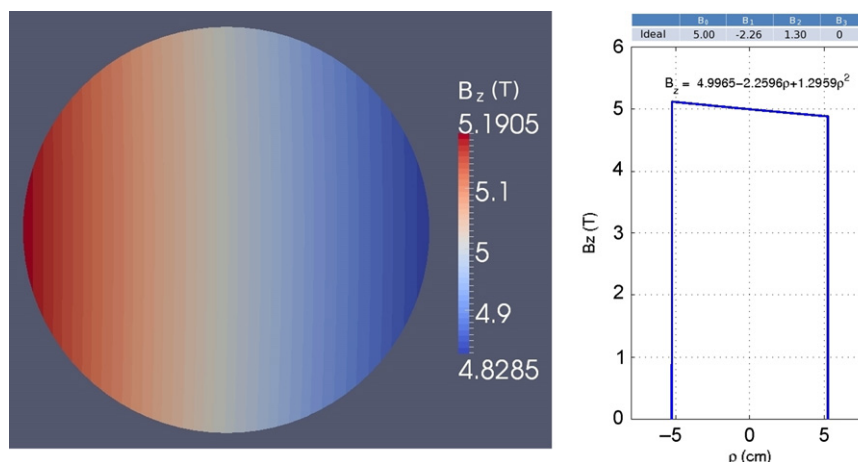


Fig. 14. Vertical magnetic fields (B_z). Left: the contour of the vertical field across the bore; Right: the profile of the vertical field on the mid-plane.

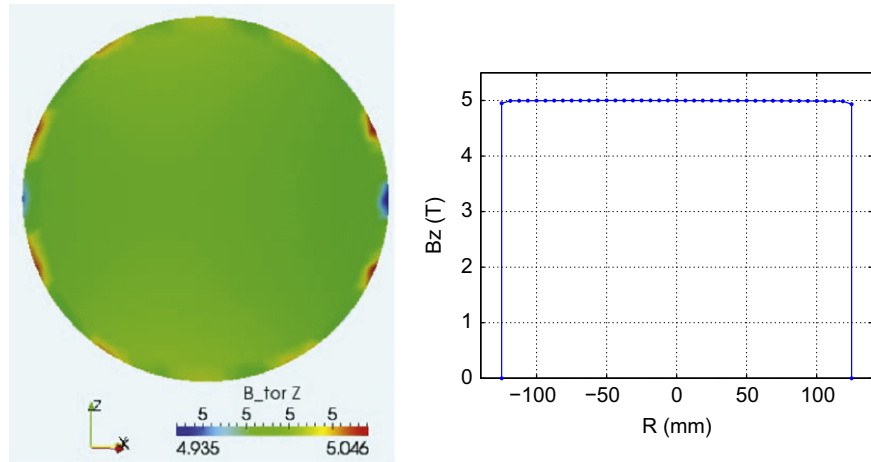


Fig. 15. A uniform dipole field (uniform color) across the bore (left) and a dipole field across the mid-plane (right). (For interpretation of the references to color in this figure legend, the reader is referred to the web version of this article.)

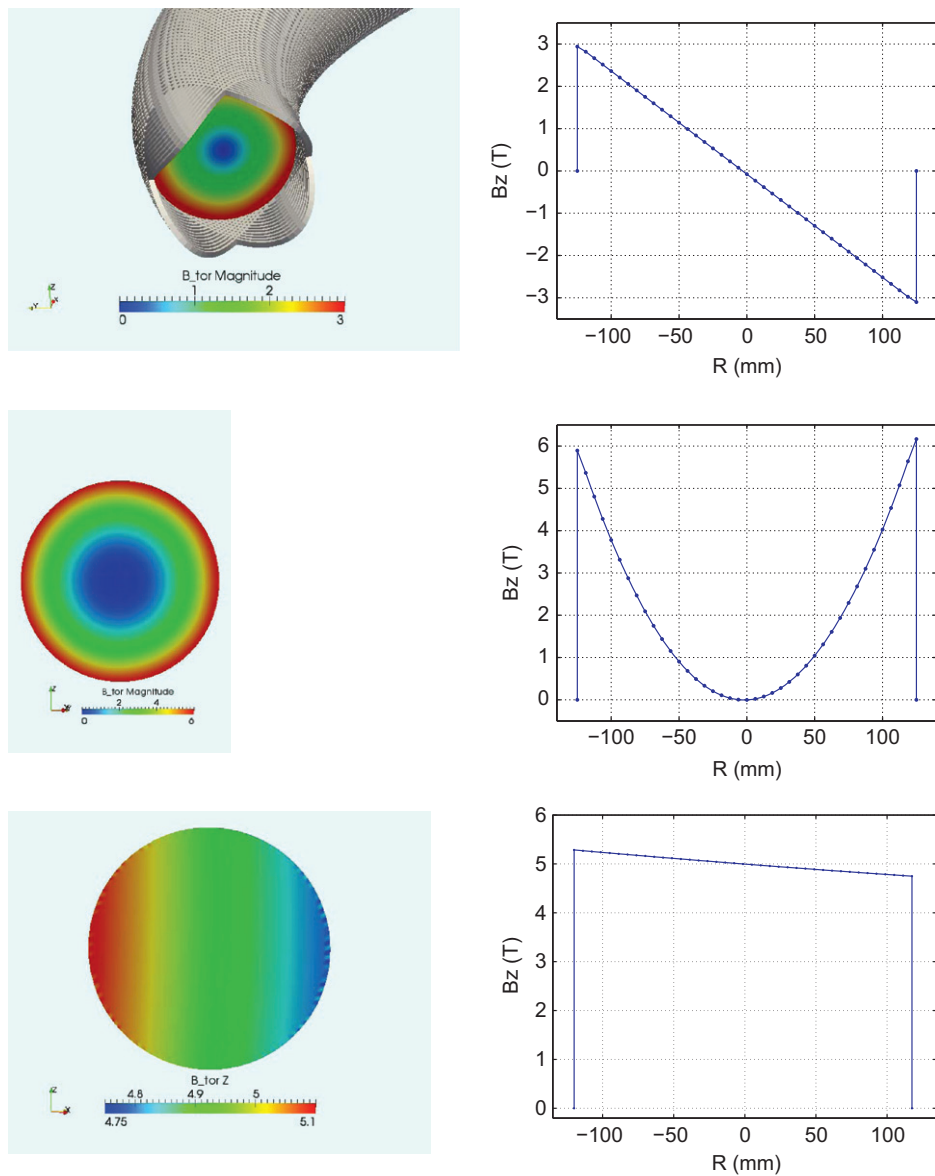


Fig. 16. A uniform quadrupole field (top), a sextupole field (middle), and a combined function dipole field superposed with a quadrupole and sextupole fields (bottom).

6.2.1. Physical interpretation

The physical interpretation of the windings is now explained using a slightly different mathematical approach to place wires based on the divergence-free relation between the current density components on the surface of a torus membrane. This approach determines a current density ratio between transverse field harmonics to that of the solenoidal (assuming a single layer) and includes an asymptotic approach of a torus towards a straight cylinder. The calculated wire path can then be used in calculating the field directly from Biot–Savart law and compared with expected harmonics. The limiting asymptotic field approximation diverts the purity of each harmonic with additional non-linear terms (usually small) that could subsequently be significantly reduced. For example a path calculated for a pure dipole term will generate higher harmonic that will be calculated and included (with an inverted sign) on a second pass, generating a revised winding set with the desired purity (Fig. 15).

The relation between the azimuthal angle ϕ around a torus (radius R_0) and the transverse angle θ around the surface of a bore (radius R) is

$$\phi = \frac{R}{R_0} \frac{2}{B_{0-sol}} \left(B_d \sin \theta + \frac{GR}{2} \sin 2\theta + \frac{SR^2}{3} \sin 2\theta + \dots \right) \quad (5)$$

where B_{0-sol} is the solenoid field (in a single layer), B_d the desired dipole field, G the gradient, S the sextupole term and so on. A second layer wound in the direction of $-\theta$ (minus theta) will reverse the solenoid field $-B_{0-sol}$ in a way that nulls the superposed solenoid field and doubles all transverse terms.

Similarly, a pure quadrupole or sextupole field can be generated using the above relation to generate the winding path and then correcting using Biot–Savart (Fig. 16). Finally a combined function magnet (as needed for an Carbon Machine) could be generated assuming several terms in the θ, ϕ relation (Fig. 16).

6.3. Improvement of the beam shape with the optimize winding

The beam scanning and beam distortion was recalculated with the optimized windings. Fig. 17 shows the beam spots in the transverse plane at the patient position obtained by using the same method described above. This figure is to be compared with Fig. 9 and one can see a significant improvement of the beam shapes.

The enhancement of the beam shape is mainly due to the removal of the sextupole in the main body. In order to see this, linear and nonlinear transfer coefficients from the scanning magnet to the patient are computed based on the particle tracking. The output phase-space coordinates of a particle can

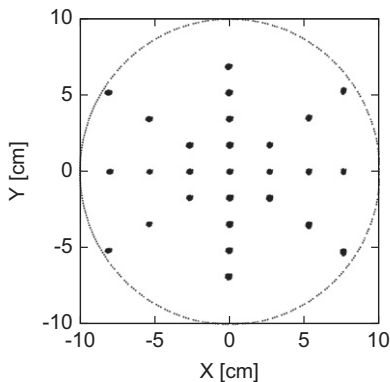


Fig. 17. Beam shapes at the patient position with optimized winding without iron.

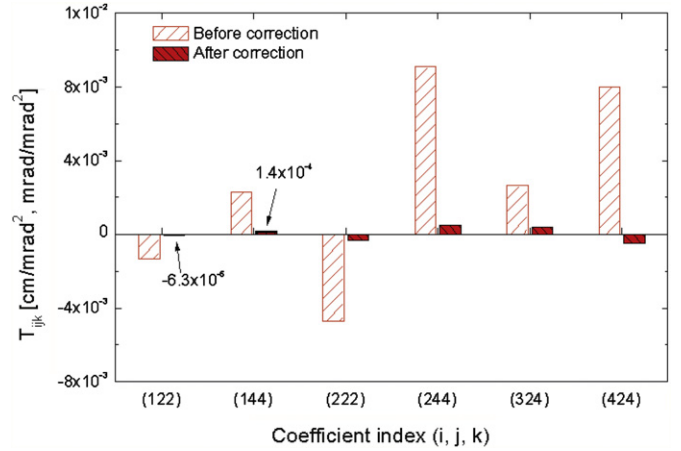


Fig. 18. Comparison of second-order transfer coefficients for old (unoptimized) and newly designed 90° magnet.

be expressed in an expanded form:

$$X_i = \sum_{j=1}^6 R_{ij} X_{j0} + \sum_{\substack{j,k \\ j \leq k}} T_{ijk} X_{j0} X_{k0} + \sum_{\substack{j,k,l \\ j \leq k \leq l}} U_{ijkl} X_{j0} X_{k0} X_{l0} + \dots \quad (6)$$

where R , T , and U are first-, second-, and third-transfer coefficients, respectively. X_{i0} and X_i are the i th phase-space coordinates at the input and output positions, respectively.

A number of specially chosen initial particles in phase space allows us to get all terms up to third-order in closed forms using the least-square minimization method. Total 121 particles (including a reference particle) are used to obtain all first-, second-, and third-order terms [22].

Fig. 18 shows six second-order transfer coefficients T_{ijk} for old (Fig. 9) and new (Fig. 17) designs. The most important terms relate the final positions in terms of the initial angles. They are the T_{122} , T_{144} , in x , and the T_{124} in y . It is seen that compared to the old design, the new design yields a significant reduction of the second-order transfer coefficients. Even in the optimized design there is still some distortion at large amplitudes that could be reduced with further optimization. Work is in progress to directly reduce the higher order terms in the transfer map.

7. Conclusion and future directions

In the paper we demonstrated that it is possible to find a winding scheme for a tilted solenoidal pair wound on a toroid that will produce the fields required for beam scanning. Our initial assessment is that this winding is physically possible and maintains tension. The coil optimization resulted in nearly linear position response to scanning magnet changes and small distortion within the scanning range. Further studies will be carried out to study the field tolerance to winding placement.

The coil optimization is just a first step in understanding the feasibility of such a magnetic system. Our plans are now to add iron and then to evaluate the stored energy, stresses, inductance (and impacts for quench protection and ramping rate limits), fast ramping and cryogenic systems. There has already been some initial estimates made indicating that the prestress requirements are at a reasonable level (less than 110 mPa).

Acknowledgements

This work was supported under Contract No. DE-AC02-05CH11231 awarded by the United States Department of Energy

to The Regents of the University of California for management and operation of the Lawrence Berkeley National Laboratory. In addition, one of the authors (M. Yoon) appreciates the partial support from the POSTECH Basic Science Research Institute Grant.

References

- [1] U. Weinrich, in: Proceedings of the 2006 European Particle Accelerator Conference, Edinburgh, Scotland, 2006, pp. 964–968.
- [2] R. Fuchs, et al., in: Proceedings of the 2004 EPAC Conference, 2004, pp. 2550–2552.
- [3] E. Pedroni, et al., Zeitschrift fur Medizinische Physik 14 (2004) 25.
- [4] M.M. Necchi, S. Savazzi, C. Viviani, J. Osorio Moreno, Functional Specifications, Union of Light Ion Centers in Europe Deliverable Report JRA6.1 2010, vol. A565, 2006, p. 430.
- [5] M. Pavlovic, E. Griesmayer, R. Seemann, Nuclear Instruments and Methods in Physics Research Section A 545 (2005) 412.
- [6] D.I. Meyer, R. Flasck, Nuclear Instruments and Methods 80 (1970) 339.
- [7] C.L. Goodzeit, M.J. Ball, R.B. Meinke, IEEE Transactions on Applied Superconductivity 13 (2) (2003) 1365.
- [8] R.B. Meinke, et al., Superconducting double-helix accelerator magnets, in: Proceedings of Particle Accelerator Conference, 2003, pp. 1996–1998.
- [9] A.V. Gavrilin, et al., IEEE Transactions on Applied Superconductivity 13 (2) (2003) 1213.
- [10] A.V. Gavrilin, et al., IEEE Transactions on Applied Superconductivity 12 (1) (2002) 465.
- [11] A.M. Akhmeteli, A.V. Gavrilin, W.S. Marshall, IEEE Transaction on Applied Superconductivity 15 (part 2) (2005) 1439.
- [12] A. Devred, et al., Superconductor Science and Technology 19 (2006) 67.
- [13] A. Devred, private communication.
- [14] R.B. Meinke, C.L. Goodzeit, M.J. Ball, IEEE Transaction on Applied Superconductivity 13 (2) (2003) 1369.
- [15] C. Goodzeit, R. Meinke, M. Ball, Combined function magnets using double-helix coils, in: Proceedings of the Particle Accelerator Conference, 2007, PAC IEEE, 2007, pp. 560–562.
- [16] S. Caspi, D.R. Dietderich, P. Ferracin, N.R. Finney, M.J. Fuery, S.A. Gourlay, A.R. Hafalia, IEEE Transaction on Applied Superconductivity 17 (part 2) (2007) 2266.
- [17] L.J. Laslett, S. Caspi, M. Helm, Particle Accelerators 22 (1987) 1.
- [18] S. Caspi, M. Helm, L.J. Laslett, IEEE Transactions on Magnetics 30 (1994) 2419.
- [19] K. Makino, M. Berz, Nuclear Instruments and Methods in Physics A 427 (1999) 338.
- [20] K. Deb, Multi-objective Optimization using Evolutionary Algorithms, John Wiley and Sons, Ltd., West Sussex, England, 2001.
- [21] <<http://scs.lbl.gov/html/Lawrencium.html>>.
- [22] M. Yoon, A Method of Computing First-, Second-, and Third-Order Transfer Coefficients for Arbitrary Fields, Technical Notes, ALS, LBNL, January 2011.